

# Opacity effects on the solar interior

## I. Solar structure

S. C. Tripathy<sup>1</sup> and J. Christensen-Dalsgaard<sup>2,3</sup>

<sup>1</sup> Udaipur Solar Observatory, Physical Research Laboratory. PO Box No. 198, Udaipur 313 001, India  
e-mail: sushant@uso.ernet.in

<sup>2</sup> Teoretisk Astrofysik Center, Danmarks Grundforskningsfond

<sup>3</sup> Institut for Fysik og Astronomi, Aarhus Universitet, DK-8000 Aarhus C, Denmark  
e-mail: jcd@obs.aau.dk

Received date; accepted date

**Abstract.** Despite recent major advances, the opacity remains a source of substantial uncertainty in the calculation of solar models, and hence of solar oscillation frequencies. Hence it is of substantial interest to investigate the sensitivity of solar structure to changes in the opacity. Furthermore, we may hope from the precise helioseismic inferences of solar structure to obtain information about possible corrections to the opacities used in the model calculation. Here we carry out detailed calculations of the influence on solar models of changes in the opacity, including also evolutionary effects. We find that over the relevant range the response of the model is approximately linear in the opacity change, allowing the introduction of *opacity kernels* relating a general opacity change to the corresponding model changes. Changes in the convection zone can be characterized entirely by the change in the initial composition and mixing length required to calibrate the model.

**Key words:** Sun: evolution – Sun: interior – Sun: oscillations – Sun: convection zone – Sun: neutrinos – stars: interior opacity

## 1. Introduction

Accurate frequency measurements of thousands of modes of solar acoustic oscillation provide detailed information on the solar interior. In order to use these frequencies to derive internal structure and dynamics of the Sun, it is crucial to understand and limit the uncertainties in the computation of solar models and mode frequencies. Furthermore, it is of considerable interest to investigate the sensitivity of solar structure to changes in the input physical parameters and properties of the solar interior. One

*Send offprint requests to:* S. C. Tripathy

of the important physical properties in solar model calculations is the opacity, which is intimately linked to the properties of the solar oscillations through its effects on the mean structure of the Sun. Here we investigate the sensitivity of solar structure to local modifications to the opacity.

Several authors have investigated the effect of opacity on the solar models and oscillation frequencies. In an early paper, Bahcall, Bahcall & Ulrich (1969) studied the sensitivity of the solar neutrino fluxes to localised changes in the opacity and equation of state and concluded that the neutrino capture rates are more sensitive to the equation of state. The effects of artificial opacity modifications on the structure of solar models and their frequencies were also examined by Christensen-Dalsgaard (1988). Constructing static models of the present Sun with an enhanced opacity near the base of the convection zone, he showed that the changes in structure and frequencies are approximately linear even to an opacity change of 60%. The linearity of the response of the model to opacity changes was later confirmed by Christensen-Dalsgaard & Thompson (1991). In a detailed investigation, Korzenik & Ulrich (1989) attempted to improve the agreement between the theoretical and observed frequencies of oscillations by determining corrections to the opacity through inverse analysis. They found that the opacity inversion can only partially resolve the discrepancy. In a similar analysis, Saio (1992) obtained opacity corrections by fitting to low-degree frequency separations and helioseismically inferred sound speeds at a few points in the model; he found that much of the discrepancy between the Sun and the model could be removed by opacity changes of up to 50%. More recently, Elliott (1995) investigated the helioseismic inverse problem as expressed in terms of corrections to the opacity. He derived kernels relating the opacity differences to the changes in frequencies, on the assumption that the change in luminosity could be ignored; he proceeded to carry out inversions for the opacity errors, based on the

observed solar oscillation frequencies, and neglecting possible changes in composition associated with the change in opacity. He found that the differences between observed and computed oscillation frequencies could be accounted for by opacity changes of up to about 5 %.

Here we carry out a detailed investigation of the sensitivity of solar structure to localised changes in the opacity, both for static and evolutionary solar models. The ultimate goal, taken up in a subsequent paper, is to determine the opacity corrections required to account for the helioseismically inferred properties of the solar interior. In general the opacity  $\kappa$  is a function of density  $\rho$ , temperature  $T$  and composition  $\{X_i\}$ . However, it is evident that information about the properties of the present Sun cannot constrain the opacity in such generality. Thus, for simplicity, we consider only opacity modifications that are functions  $\delta \log \kappa(T)$  of temperature alone, log being the logarithm to base 10. If the opacity correction is sufficiently small that higher-order terms can be neglected, the response of any quantity  $F$  related to solar structure can be expressed in terms of a differential kernel  $K_F$  as

$$\frac{\delta F}{F} = \int K_F(T) \delta \log \kappa(T) d \log T. \quad (1)$$

Here for simplicity we estimate the kernels from

$$K_F(T_0) = \frac{(\delta F/F)(T_0)}{\int \delta \log \kappa(T) d \log T}, \quad (2)$$

where  $\delta F$  is the change corresponding to a suitably change  $\delta \log \kappa$  localised at  $T = T_0$ . Relations similar to Eq. (1) form the basis of inverse analysis (Gough 1985): if  $\delta F$  is the difference between the observed and theoretical frequencies, Eq. (1) can in principle be inverted to determine corrections to the opacity in the model (Korzennik & Ulrich 1989; Saio 1992; Elliott 1995). The kernels also provide a powerful visualization of the response in a given physical quantity of the solar model to a small perturbation in the input physics. As an example of this we evaluate kernels relating opacity changes to the structural differences in the solar model, the neutrino fluxes, and the small frequency separation between low-degree modes.

## 2. Procedure

To illustrate the sensitivity of the models to opacity changes we have computed extensive sets of comparatively simple models. These were based on the OPAL opacity tables (Iglesias, Rogers & Wilson 1992), the Eggleton, Faulkner & Flannery (1973) equation of state, and nuclear reaction parameters from Parker (1986) and Bahcall & Ulrich (1988). Convection was treated with the mixing-length formulation of Böhm-Vitense (1958). The neutrino capture rates for the  $^{37}\text{Cl}$  and  $^{71}\text{Ga}$  experiments were obtained with the cross-sections given by Bahcall (1989). The heavy-element abundance  $Z$  was 0.01895. All models were calibrated to a fixed radius ( $6.9599 \times 10^{10}$  cm) and luminosity ( $3.846 \times 10^{33}$  erg s $^{-1}$ ) at the assumed solar age of

$4.6 \times 10^9$  years by adjusting the mixing-length parameter  $\alpha_c$  and the composition. Diffusion and gravitational settling were ignored. Details of the computational procedure were described by Christensen-Dalsgaard (1982).

It should be noted that our models are somewhat simplified, particularly in the choice of equation of state and the neglect of settling, compared with present state-of-the-art solar models (for a review see, for example, Christensen-Dalsgaard *et al.* 1996). Thus the values of the model parameters quoted, e.g., in Table 1 cannot be regarded as representative of the actual solar structure. However, we are here concerned with the *differential* effects on the models of changes to the opacity; for this purpose, the present simplified physics is entirely adequate.

We have considered two types of models: static models of the present Sun and proper evolution models, evolved from a chemically homogeneous initial Zero-Age Main-Sequence (ZAMS) model. In the static models, the hydrogen profile  $X(q)$  where  $q = m/M$  ( $m$  being the mass interior to the given point and  $M$  is the total mass of the Sun), was obtained by scaling by a constant factor the profile  $X_r(q)$ , obtained from a complete evolution model:  $X(q) = \chi X_r(q)$ , (3)

where  $\chi$  was adjusted to fit the solar luminosity. In the evolution models the calibration to solar luminosity was achieved by adjusting the initial helium abundance  $Y_0$ .

The sensitivity of solar structure to opacity was investigated by increasing  $\kappa$  in a narrowly confined region near a specific temperature  $T_0$  according to

$$\log \kappa = \log \kappa_0 + f(T_0), \quad (4)$$

where  $\kappa_0$  is the opacity as obtained from the opacity tables;  $T_0$  was varied over the temperature range of the model. The function  $f(T_0)$  has the form

$$f(T_0) = A \exp \left[ - \left( \frac{\log T - \log T_0}{\Delta} \right)^2 \right], \quad (5)$$

where the constants  $A$  and  $\Delta$  determine the magnitude and width of the opacity modification. Henceforth the models computed with the same input physics but without opacity modifications will be referred to as reference models whereas the perturbed ones will be referred as modified models.

The detailed response of the oscillation frequencies to the opacity modifications will be considered separately. However, the importance of the small frequency separation as a diagnostics of the solar core motivates that we include it here, for comparison with the response of the neutrino flux. We characterize the separation, averaged over radial order  $n$  and degree  $l$ , by the parameter  $D_0$  defined by

$$\langle \nu_{nl} - \nu_{n-1, \ell+2} \rangle_{n,l} \simeq (4\ell + 6) D_0, \quad (6)$$

where asymptotically

$$D_0 \simeq - \frac{1}{4\pi^2(n_0 + 1/4 + \beta)} \int_0^R \frac{dc}{dr} \frac{dr}{r}. \quad (7)$$

**Table 1.** Properties of static solar models. Here  $X_0$  is the initial hydrogen abundance,  $\alpha_c$  is the mixing-length parameter,  $d_{cz}/R$  is the depth of the convection zone in units of photospheric radius  $R$ ,  $T_c$  and  $X_c$  are central temperature and hydrogen abundance of the model of the present Sun, and the last three columns give the neutrino capture rates in the  $^{37}\text{Cl}$  and  $^{71}\text{Ga}$  experiments, and the flux of  $^8\text{B}$  neutrinos.

Model	$A$	$X_0$	$\alpha_c$	$d_{cz}/R$	$T_c$ ( $10^6\text{K}$ )	$X_c$	Neutrino flux		
							$^{37}\text{Cl}$ (SNU)	$^{71}\text{Ga}$ (SNU)	$^8\text{B}$ $10^6\text{cm}^{-2}\text{s}^{-1}$
S0	0.0	0.6978	1.8098	0.2739	15.604	0.3383	8.092	132.02	5.747
SA	0.02	0.6972	1.8038	0.2733	15.601	0.3380	8.073	131.97	5.730
SB	0.1	0.6948	1.7813	0.2709	15.589	0.3369	8.006	131.84	5.670
SC	0.2	0.6920	1.7561	0.2681	15.576	0.3355	7.939	131.72	5.608

Here  $n_0$  is a suitable reference order,  $\beta$  is a constant predominantly related to the structure of the outer parts of the model, and  $c$  is the sound speed. Details of the calculation of the oscillation frequencies and the evaluation of the average in Eq. (6) were given by Christensen-Dalsgaard & Berthomieu (1991). The fit to the frequencies included modes with  $l = 0 - 4$  and radial order such that  $17 \leq n + l/2 \leq 29$ ;  $n_0$  was chosen to be 23.

### 3. Results

#### 3.1. Linearity of the response

The linearity of the response of model parameters to the opacity modifications was tested by constructing static models with  $A = 0.02, 0.1$  and  $0.2$  (note that  $A = 0.1$  corresponds to a maximum change in opacity of 26%). The modifications were centred at  $\log T_0 = 7$ , and the width was  $\Delta = 0.02$  (here and in the following  $T$  and  $T_0$  are measured in K). The properties of the reference and modified models are presented in Table 1. It is evident that the changes in opacity required fairly substantial changes in the composition and mixing-length parameter to calibrate the model to obtain the correct luminosity and radius, and led to a significant change in the depth of the convection zone.

Fig. 1 shows the change in sound speed, temperature and density resulting from the opacity change with  $A = 0.1$  and  $0.2$ , the differences for  $A = 0.2$  being scaled by  $1/2$  to test linearity. Even though the curves do not coincide precisely, the model changes are approximately linearly related to even quite substantial changes in  $\log \kappa$ , as was also found in earlier investigations. We have in addition confirmed that the changes are relatively insensitive to the width  $\Delta$ , provided the integrated modification  $\int \delta \log \kappa d \log T$  is kept fixed.

A requirement for linearity is that the model does not become convectively unstable at the location where the opacity is modified. This constraint can approximately be formulated as

$$(\delta \ln \kappa)_{\max} = (\ln 10) A < \frac{\nabla_{\text{ad}}}{\nabla} - 1, \quad (8)$$

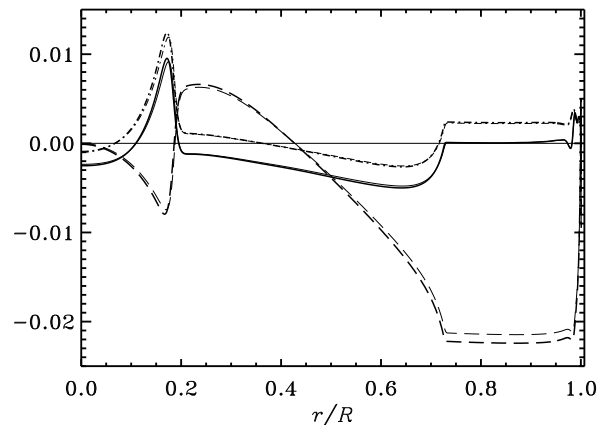


**Fig. 1.** Differences at fixed fractional radius  $r/R$  between static modified models SB and SC and the reference model S0, in the sense (modified model) – (reference model). The heavy lines show results for  $A = 0.1$  and the thin lines results for  $A = 0.2$ , multiplied by  $1/2$  to illustrate the extent to which the response is linear. The following differences are illustrated:  $\delta_r \ln c^2$  (solid line);  $\delta_r \ln \rho$  (long-dashed line); and  $\delta_r \ln T$  (dash-dotted line),  $\ln$  being the natural logarithm

where  $\nabla = d \ln T / d \ln p$  and  $\nabla_{\text{ad}}$  is its adiabatic value, both evaluated in the reference model. We note that this constraint is only barely satisfied for  $A = 0.2$  and  $\log T_0 = 7$ : had we used  $A = 0.3$  instead, the region around the modification would have become convectively unstable and the structure of the model would have been drastically altered.

In the following we consider modifications computed using  $A = \Delta = 0.02$ , corresponding to Model SA in Table 1; this is sufficiently localized to represent the linear response of opacity modifications confined to very narrow local regions, similar to delta functions. Furthermore, this value of  $A$  ensures that the constraint (8) is satisfied, except in a few cases in the core during early stages of evolution, of little significance to the structure of the model of the present Sun. Specifically, a small short-lived ini-

tial convective core appeared in the evolution calculations for  $7.11 < \log T_0 < 7.15$ ; to avoid problems with non-linearities we simply suppressed the mixing of the composition of the core in these cases.

### 3.2. Model differences

Changes in static solar models in response to opacity modifications at various locations are illustrated in Fig. 2, in terms of differences ( $\delta_r$ ) between the modified and reference models at fixed fractional radius  $r/R$ . Corresponding results for evolution models are shown in Fig. 3. The changes in the initial hydrogen abundance  $X_0$  and mixing-length parameter  $\alpha_c$  required to calibrate the models are shown in Fig. 4 as functions of  $\log T_0$ , together with other overall properties of the models. It is apparent that  $\delta_r \ln T$ ,  $\delta_r \ln c$  and  $\delta_r \ln \rho$  behave almost like step functions at the location  $T = T_0$  of the imposed opacity change; furthermore  $\delta_r \ln T$  and  $\delta_r \ln c$  are largely localized near this point. On the other hand,  $\delta_r \ln p$  has a gentler behaviour. These properties are investigated in more detail in Sect. 4.1 below.

Interestingly, the central temperature  $T_c$  depends in a non-monotonic fashion on  $\log T_0$ ,  $\delta \ln T_c$  being even slightly negative for  $\log T_0 \simeq 7.0$  (see Fig. 4a). The reason for this behaviour is not obvious, although it may be related to the steep decrease in  $\delta_r \ln T$  with increasing  $T$ , and hence decreasing  $r$ , below the region of immediate opacity modification (see also Sect. 4.1). The generation of the high-energy neutrinos is strongly coupled to  $T_c$ , and indeed the changes in the neutrino fluxes closely follow  $\delta \ln T_c$  (cf. Fig. 4b). In particular, there is also a slight decrease in the neutrino flux for an opacity increase near  $\log T_0 \simeq 7$ . This is in contrast to the calculation of Bahcall *et al.* (1969) where the flux in models with increased opacity is higher than in the reference model at all values of  $T_0$  (cf. Fig. 1 of their paper). However, we note that Bahcall *et al.* used an opacity modification with a width in  $\log T$  approximately six times as large as in our case; this is likely to have suppressed the finer structure in the dependence of the neutrino flux on  $T_0$ .

Opacity increases generally lead to a decrease in the hydrogen abundance. Indeed, an increase in opacity would tend to decrease the luminosity; it follows from homology scaling (e.g. Kippenhahn & Weigert 1990) that this can be compensated for by an increase in the mean molecular weight, i.e., a decrease in  $X_0$ . When the opacity change is localized to the outer parts of the radiative region, the changes in the core of the model, and hence in the value of  $X_0$  required for calibration, become very small.

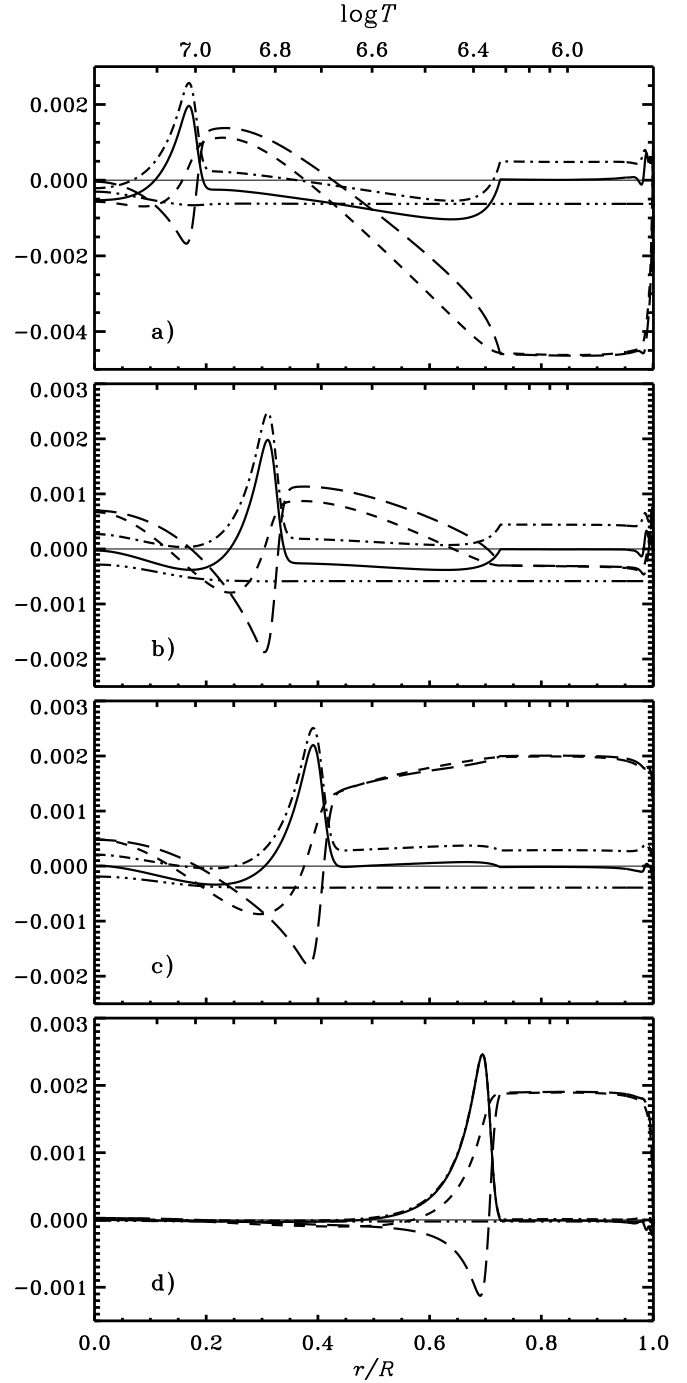


**Fig. 2.** Differences between modified static models and the reference model S0 in the sense (modified model) – (reference model). The modified models correspond to the following locations of the opacity increases: **a**  $\log T_0 = 7.0$ ; **b**  $\log T_0 = 6.8$ ; **c**  $\log T_0 = 6.7$ ; **d**  $\log T_0 = 6.36$ . The variables shown are:  $\delta_r \ln c^2$  (solid line);  $\delta_r \ln p$  (short-dashed line);  $\delta_r \ln \rho$  (long-dashed line);  $\delta_r \ln T$  (dash-dotted line); and  $\delta_r X$  (dash-triple-dotted line)

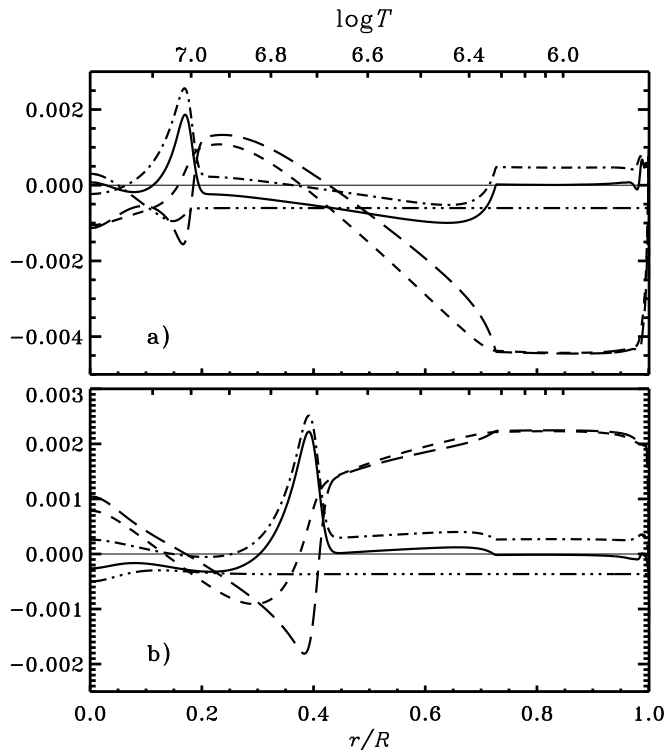


**Fig. 3.** Differences between modified evolution models and the corresponding reference model, in the sense (modified model) – (reference model). The modified models correspond to the following locations of the opacity increases: **a**  $\log T_0 = 7.0$ ; **b**  $\log T_0 = 6.7$ . The line styles have the same meaning as in Fig. 2

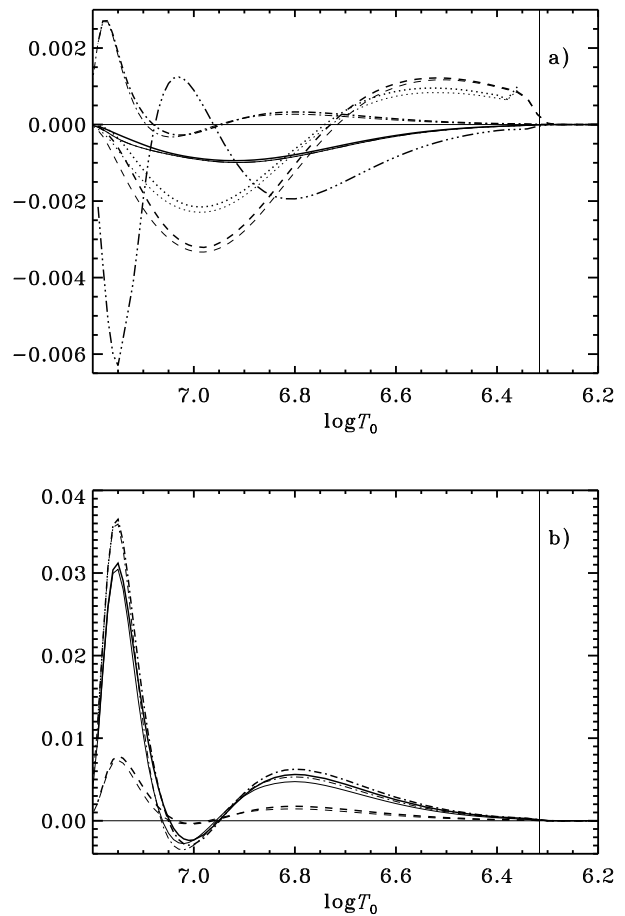


**Fig. 4.** Responses of various global model quantities, as a function of the location  $T_0$  of the opacity modification, shown in the sense (modified model) – (reference model). Thin lines correspond to static models and heavy lines to evolution models. The thin vertical line corresponds to the temperature at the base of the convection zone in the reference model. **a** Relative changes in central temperature  $T_c$  (dash-dotted line), depth of the convection zone (dotted line), and mixing-length parameter  $\alpha_c$  (dashed line), initial hydrogen abundance  $X_0$  (solid line) and central hydrogen abundance  $X_c$  (dash-triple-dotted line). (Note that for the static models, the relative changes in  $X_0$  and  $X_c$  are identical.) **b** Relative changes in the  $^{37}\text{Cl}$  and  $^{71}\text{Ga}$  capture rates (solid and dashed lines, respectively) and the flux of  $^8\text{B}$  neutrinos (dot-dashed line)

Fig. 4, and a comparison of Figs 2 and 3, show substantial differences between the static and the evolution models in the changes in  $X$  in the core of the model. In the static case,  $\delta_r X$  is determined by the scaling in Eq. (3), together with the change in mass fraction  $q$  at fixed  $r$ . The overall effect is that the change is somewhat smaller in the core than elsewhere. For the evolution models, on the other hand, the change in the initial abundance is modified by the change in the rate of nuclear burning, which in turn depends predominantly on the change in temperature. As a result, the change in the central hydrogen abundance  $X_c$  generally reflects the change in the central temperature  $T_c$ , as is evident from Fig. 4. This difference between static and evolution models in the behaviour of the hydrogen abundance in the core leads to differences in the core response for other model variables, as is clear from a comparison of Figs 2 and 3; on the other hand, there is striking similarity between the results for static and evolution models elsewhere, indicating that the use of static models is indeed a useful and computationally efficient technique for investigating the response of the models to changes in the physics.

The behaviour of  $\delta_r \ln p$  and  $\delta_r \ln \rho$ , particularly in the convection zone, shows a striking variation with  $T_0$ , the differences in the outer parts of the model changing sign for  $\log T_0 \simeq 6.74$ . As discussed in Sect. 4.2 below, these changes are related to the complex behaviour of  $\alpha_c$  and result from the matching between the convection zone and the radiative interior, and the calibration of the model to fixed radius.

We finally note from Fig. 4 that, as expected, the model differences are negligible for opacity modifications confined essentially to the convection zone, corresponding to  $\log T_0 \lesssim 6.25$ ; this evidently follows from the fact that the structure of the nearly adiabatic part of the convection zone is independent of opacity.

#### 4. Analysis of the model response

In general, the response of the model to changes in aspects of the physics is quite complex, as is also apparent from the results presented so far. However, it is possible to obtain some understanding of important aspects of the model changes from relatively simple analyses. Here we consider the response in the vicinity of the imposed opacity change, and the behaviour of changes in the convection zone.

##### 4.1. Local response of temperature and pressure

The numerical results presented in Sect. 3.2 indicate a great deal of regularity in the response near the point where the opacity modification is made. Some properties of this behaviour can be understood quite simply in terms

of the perturbed equations of stellar structure. For simplicity, we assume that the change in local mass and luminosity can be neglected; the latter assumption is certainly satisfied outside the nuclear-burning region, where the luminosity is fixed by the calibration, while we have found from the numerical results that the perturbation in mass is comparatively small. Also, we evidently consider only the radiative part of the star. Under these assumptions the model response is determined by just the equations of hydrostatic equilibrium and radiative energy transport which, upon linearization, yield

$$\frac{d}{dr} \frac{\delta_r p}{p} = \frac{d \ln p}{dr} \left( \frac{\delta_r \rho}{\rho} - \frac{\delta_r p}{p} \right), \quad (9)$$

and

$$\frac{d}{dr} \frac{\delta_r T}{T} = \frac{d \ln T}{dr} \left[ \left( \frac{\delta \kappa}{\kappa} \right)_{\text{int}} + (\kappa_\rho + 1) \frac{\delta_r \rho}{\rho} + (\kappa_T - 4) \frac{\delta_r T}{T} \right]. \quad (10)$$

In Eq. (10)  $\kappa_\rho = (\partial \ln \kappa / \partial \ln \rho)_T$  and  $\kappa_T = (\partial \ln \kappa / \partial \ln T)_\rho$ , and  $(\delta \kappa / \kappa)_{\text{int}}$  is the intrinsic opacity modification, corresponding to Eq. (5). In Eq. (10) we neglected the effect on the opacity of the change in composition, required by the calibration of the model; this change is also found to be small, compared with the dominant effects. Still neglecting effects of composition and assuming the ideal gas law, the modifications in pressure, density and temperature are related by

$$\frac{\delta_r p}{p} = \frac{\delta_r \rho}{\rho} + \frac{\delta_r T}{T}. \quad (11)$$

It is evidently possible to carry out a complete description of the modifications to the model through numerical solution of these equations, with appropriate boundary conditions; the analysis should then include also the changes in mass and luminosity, as described by the linearized versions of the relevant equations, and the effect on the composition. Here, however, we approximate the equations further, in order to obtain a rough analytical solution which may be used to interpret the numerical results. From Eq. (10) it is evident that an intrinsic modification  $(\delta \kappa / \kappa)_{\text{int}}$  approximating a delta function induces a step function in  $\delta_r T / T$ , while, from Eqs (9) and (11),  $\delta_r p / p$  results from an integration over this step function. Thus it is plausible, as confirmed by the numerical results, that near the modification  $\delta_r T / T$  is substantially larger than  $\delta_r p / p$ . Consequently we neglect  $\delta_r p / p$  in Eq. (11) to obtain  $\delta_r \rho / \rho \simeq -\delta_r T / T$  and hence, from Eq. (10),

$$\frac{d}{d \ln T} \frac{\delta_r T}{T} + \zeta \frac{\delta_r T}{T} = \left( \frac{\delta \kappa}{\kappa} \right)_{\text{int}}, \quad (12)$$

where  $\zeta = 5 + \kappa_\rho - \kappa_T$ . We assume that  $\kappa_\rho$  and  $\kappa_T$  are approximately constant, and take as boundary condition

that  $\delta_r T/T = (\delta_r T/T)_s$  at a suitable reference temperature  $T_s < T_0$ . Then the solution to Eq. (12) is

$$\frac{\delta_r T}{T} = \begin{cases} \left(\frac{T_s}{T}\right)^\zeta \left(\frac{\delta_r T}{T}\right)_s & \text{for } T < T_0, \\ \left(\frac{T_s}{T}\right)^\zeta \left(\frac{\delta_r T}{T}\right)_s + K_0 \left(\frac{T_0}{T}\right)^\zeta & \text{for } T > T_0, \end{cases} \quad (13)$$

where

$$K_0 = \int \left(\frac{\delta\kappa}{\kappa}\right)_{\text{int}} d \ln T. \quad (14)$$

The exponent  $\zeta$  is large: at a typical point in the solar radiative interior,  $\kappa_T \simeq -2.5$  and  $\kappa_\rho \simeq 0.5$ , so that  $\zeta \simeq 8$ . Consequently, the term in  $(T_s/T)^\zeta$  decreases very rapidly with increasing depth and, as a first approximation,  $\delta_r T/T \simeq K_0(T_0/T)^\zeta$  for  $T > T_0$  and zero otherwise.

To estimate  $\delta_r p/p$  we write Eq. (9) as, using Eq. (11),

$$\frac{d}{d \ln T} \frac{\delta_r p}{p} = -\nabla^{-1} \frac{\delta_r T}{T}, \quad (15)$$

where  $\nabla = d \ln T / d \ln p$ . Assuming  $\nabla$  to be roughly constant over the relevant region and using the approximate solution for  $\delta_r T/T$ , we obtain

$$\frac{\delta_r p}{p} \simeq \begin{cases} \left(\frac{\delta_r p}{p}\right)_0 & \text{for } T < T_0, \\ \left(\frac{\delta_r p}{p}\right)_0 + \frac{K_0}{\zeta \nabla} \left[ \left(\frac{T_0}{T}\right)^\zeta - 1 \right] & \text{for } T > T_0, \end{cases} \quad (16)$$

where  $(\delta_r p/p)_0$  is the value of  $\delta_r p/p$  at  $T = T_0$ .

To test these expressions, we consider in Fig. 5 the case, already presented in Fig. 2b, of a static model modified with  $\log T_0 = 6.8$ ; since the analytical solutions depend predominantly on temperature, we show the results as a function of  $\log T$ , rather than  $r/R$ . The analytical solution for  $\delta_r T/T$  is clearly in good agreement with the numerical results; in particular, the rapid decrease, as  $T^{-\zeta}$ , for  $T > T_0$  accounts for the localized nature of the temperature modification. The fit is rather less satisfactory for  $\delta_r p/p$ , although the analytical solution approximately recovers the magnitude of the variation in the vicinity of  $T = T_0$ ; in fact, it is plausible that the neglect of the finite extent of  $(\delta\kappa/\kappa)_{\text{int}}$ , the neglect of the change in composition and the assumption that  $\nabla$  is constant are of doubtful validity in this case. Even so, the analytical solutions do provide some insight into the nature of the model response.

We finally note that the change in sound speed is given by

$$\begin{aligned} \delta_r \ln c^2 &= \delta_r \ln \gamma_1 + \delta_r \ln \left(\frac{p}{\rho}\right) \\ &\simeq \delta_r \ln \gamma_1 + \delta_r \ln T - \delta_r \ln \mu, \end{aligned} \quad (17)$$

where in the last equality the ideal gas law was assumed; here  $\gamma_1 \equiv (\partial \ln p / \partial \ln \rho)_s$ , the derivative being taken at constant specific entropy  $s$ , and  $\mu$  is the mean molecular weight. Outside ionization zones of abundant elements,

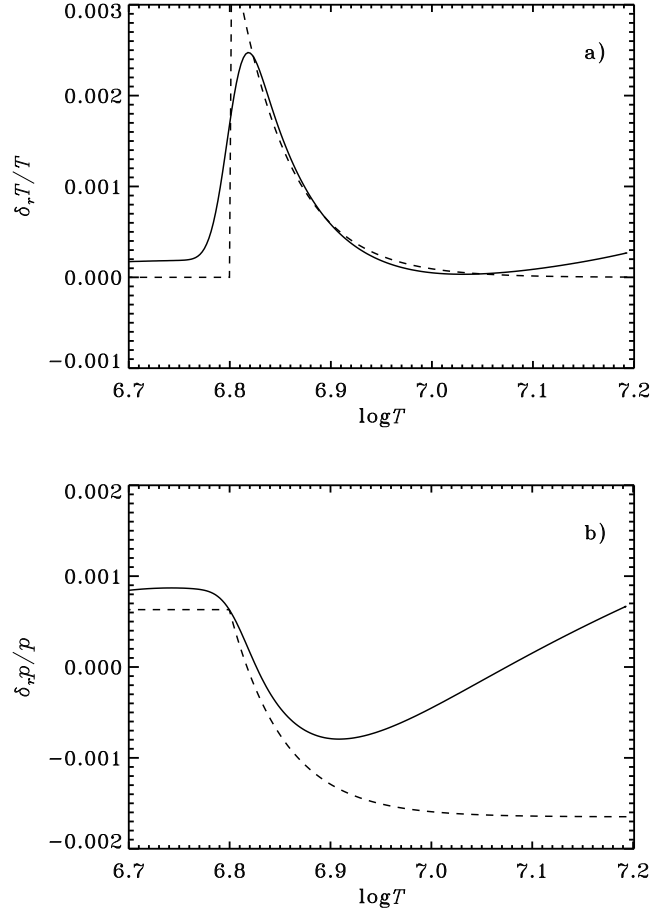


**Fig. 5.** Comparisons of actual model differences (solid lines) with analytical approximations (dashed lines), for a static model with  $\log T_0 = 6.8$ ,  $A = 0.02$  and  $\Delta = 0.02$ ; to illustrate the behaviour of the solution, position in the model is indicated by  $\log T$ . **a** Relative difference  $\delta_r T/T$  in temperature; the analytical solution was obtained from Eqs (13) and (14), neglecting the term in  $(\delta_r T/T)_s$ . **b** Relative difference  $\delta_r p/p$  in pressure; the analytical solution was obtained from Eqs (16), fitting  $(\delta_r p/p)_0$  to the numerical solution at the location  $T = T_0$  of the opacity modification

$\delta_r \ln \gamma_1$  can be approximately neglected; also,  $\delta_r \ln \mu$  is almost constant, except in the core where the composition has been altered by nuclear burning. As a result, as a first approximation  $\delta_r \ln c^2$  is obtained from  $\delta_r \ln T$  by a constant shift, as is indeed observed in Figs 2 and 3.

#### 4.2. Model differences in the convection zone

The bulk of the convection zone is very nearly adiabatically stratified; hence its structure depends only on the equation of state, the composition and the (constant) specific entropy  $s$ . Indeed, it is evident from Fig. 4 that the

model is insensitive to the opacity in the convection zone. Assuming that the physics of the atmosphere is given,  $s$  is determined, within mixing-length theory, by the mixing-length parameter  $\alpha_c$ . If, as in the calculations presented in Sect. 3, we also assume that the equation of state and the heavy-element abundance  $Z$  are fixed, the structure of the adiabatic part of the convection zone is then essentially characterized by  $\alpha_c$  and the envelope hydrogen abundance  $X_s$ . Some simple properties of such convective envelopes are discussed in the Appendix.

For model changes so small that the linear approximation is valid, the difference in any quantity  $\phi$  may be expressed in terms of the changes  $\delta X_s$  and  $\delta \alpha_c$  in  $X_s$  and  $\alpha_c$ , as

$$\delta_r \phi \simeq \left( \frac{\partial \phi}{\partial X_s} \right)_{\alpha_c; r} \delta X_s + \left( \frac{\partial \phi}{\partial \alpha_c} \right)_{X_s; r} \delta \alpha_c. \quad (18)$$

The partial derivatives in Eq. (18) may be estimated from differences between envelope models differing only in  $X_s$  or  $\alpha_c$  as, for example  $(\partial \phi / \partial X_s)_{\alpha_c; r} \simeq \delta_r \phi / \delta X_s$ . Here we consider three envelope models constructed using the same input physics as for the complete models described earlier, but with prescribed values of  $X_s$  and  $\alpha_c$ . Some properties of the models are listed in Table 2. In particular,  $K$  is the value of the constant in the adiabatic relation between  $p$  and  $\rho$  [cf. Eq. (A3) in the Appendix], averaged over the lower part of the convection zone, with  $r \leq 0.8R$ . The resulting derivatives, in the outer parts of the convection zone, are shown in Fig. 6; at greater depth the derivatives of  $\ln c^2$  are very small, and the derivatives of  $\ln \rho$  are essentially constant, in accordance with the discussion in the Appendix [cf. in particular Eq. (A6)].

For the models computed with changes in the internal opacity, the changes in  $\alpha_c$  and  $X_s$  arise from the calibration to fixed radius and luminosity. More precisely,  $X_s$  is essentially determined by the condition that the luminosity is fixed and, given  $X_s$ ,  $\alpha_c$  is determined such as to ensure a continuous match at the base of the convection zone, with a fixed surface radius. Given the partial derivatives determined from the envelope calculations, we may test Eq. (18) by comparing actual differences found in Sect. 3, resulting from opacity modifications, with those obtained from Eq. (18) with the changes in  $X_s$  and  $\alpha_c$  shown in Fig. 4a. Results for static models are shown in Figs 7 and 8. It is evident from Fig. 7, for  $\log T_0 = 7.0$ , that the simple relation (18) reproduces quite accurately the details of the sound-speed changes in the hydrogen and helium ionization zones. Also, the dominant contribution in this case clearly results from the change in  $\alpha_c$ .

Fig. 8 shows the changes in squared sound speed and density at  $r = 0.99R$ , as well as the contributions from the changes in  $\alpha_c$  and  $X_s$ , as a function of  $\log T_0$ . The dependence of the individual contributions clearly follows the variation of  $\delta \alpha_c$  and  $\delta X_s$ , shown in Fig. 4a. In particular, the complex behaviour of  $\delta \alpha_c$  is reflected in a corresponding behaviour of  $\delta_r \ln c^2$  and  $\delta_r \ln \rho$ , including the changes

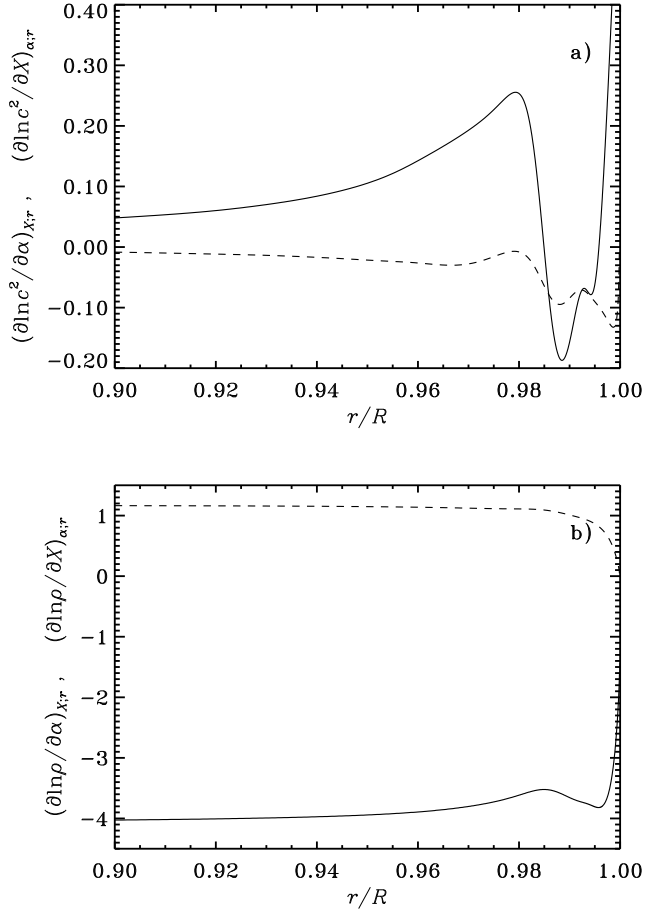


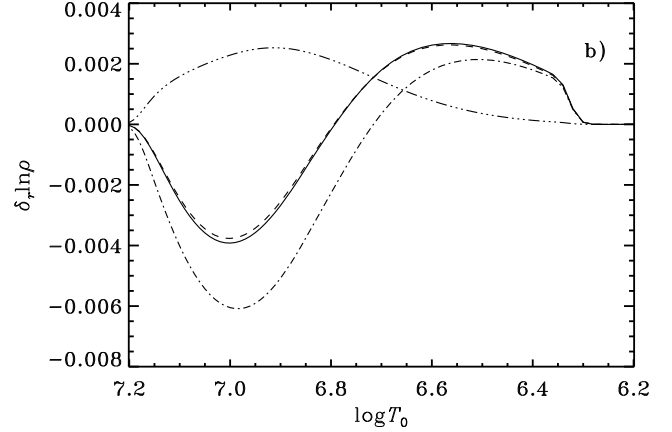
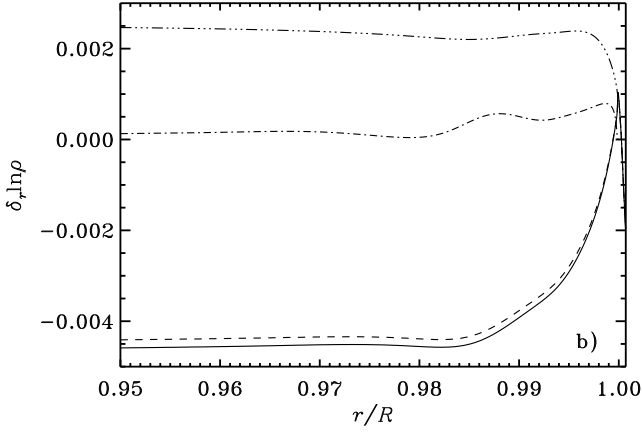
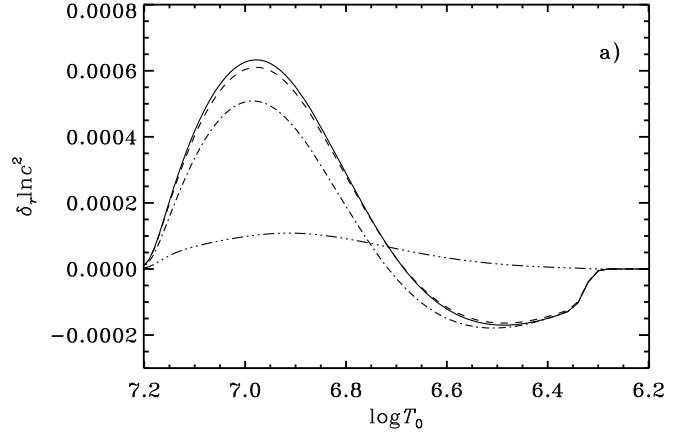
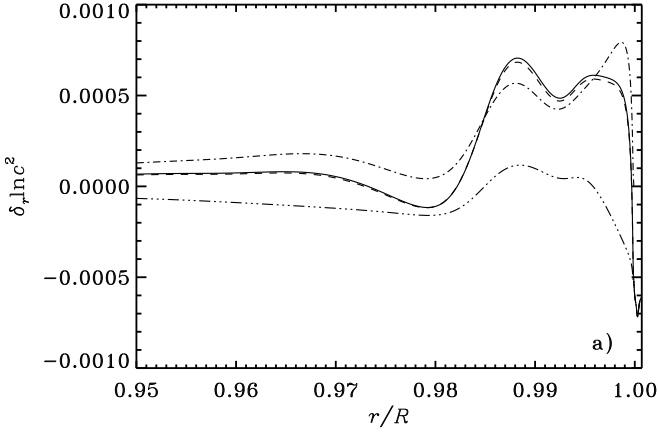
**Fig. 6.** Estimated partial derivatives of model quantities in the outer parts of the convection zone, with respect to the envelope hydrogen abundance  $X_s$  (solid lines) and the mixing-length parameter  $\alpha_c$  (dashed lines). **a** Derivatives of squared sound speed. **b** Derivatives of density

in sign for  $6.7 \leq \log T_0 \leq 6.8$ . For opacity changes closer to the base of the convection zone, the model differences are dominated by the change in  $\alpha_c$ , the contributions from the change in  $X_s$  becoming negligible. The main reasons for these variations are not obvious; however, it seems likely that the behaviour in the radiative interior (cf. Fig. 2) causes the change of sign in  $\delta_r p/p$  and  $\delta_r \rho/\rho$  at the base of the convection zone, as the location of the opacity modification moves closer to the surface. Since  $\delta_r p/p$  is directly linked to the change in the polytropic constant  $K$  by Eq. (A6), and hence to the change in  $\alpha_c$  by Eq. (A10) this is the probable cause of the change in  $\alpha_c$  and hence, by Eq. (A12), in the depth of the convection zone (see also Fig. 4). In turn, the depth of the convection zone largely controls the behaviour of  $\delta_r \ln T$  and  $\delta_r \ln c^2$  in the outer parts of the radiative region: For  $\log T_0 \gtrsim 6.74$ , the convection zone is shallower in the modified model than in the reference model. Consequently, the temperature and



**Table 2.** Properties of the envelope models.  $X_s$  is the envelope hydrogen abundance,  $p_{cz}$  is the pressure at the base of the convection zone and  $K$  is defined by the adiabatic relation (A3)

Model No.	$X_s$	$\alpha_c$	$d_{cz}/R$	$p_{cz}$ ( $\text{dyn cm}^{-2}$ )	$K$ (cgs)
En1	0.697867	1.81586	0.274105	$4.44746 \cdot 10^{13}$	$9.52969 \cdot 10^{14}$
En2	0.697867	1.84273	0.277000	$4.75692 \cdot 10^{13}$	$9.33427 \cdot 10^{14}$
En3	0.702867	1.81586	0.273757	$4.34019 \cdot 10^{13}$	$9.65974 \cdot 10^{14}$

**Fig. 7.** Differences in squared sound speed (panel a) and density (panel b) in the upper part of the convection zone, for a static model modified at  $\log T_0 = 7.0$ . The solid line shows the computed difference, from Fig. 2a, the dash-dot and dash-triple-dot lines show the contributions in Eq. (18) from  $\delta\alpha_c$  and  $\delta X_s$ , respectively, and the dashed line shows the sum of these contributions**Fig. 8.** Differences in squared sound speed (panel a) and density (panel b) at  $r = 0.99R$  in modified static models, as a function of the location  $\log T_0$  of the opacity modification. The same line styles as in Fig. 7 have been used

sound-speed gradients are less steep in the modified model just beneath the convection zone; since, as argued in the Appendix, the sound-speed difference is very small in the lower parts of the convection zone, this leads to a negative sound-speed difference in that part of the radiative

interior which lies outside the opacity modification. This trend is reversed for  $\log T_0 \lesssim 6.74$ .

## 5. Tests of the opacity kernels

As indicated by Eq. (1), the sensitivity of a physical quantity to the opacity perturbations can be measured by opacity kernels. In this section we present examples of such kernels. We furthermore test the accuracy with

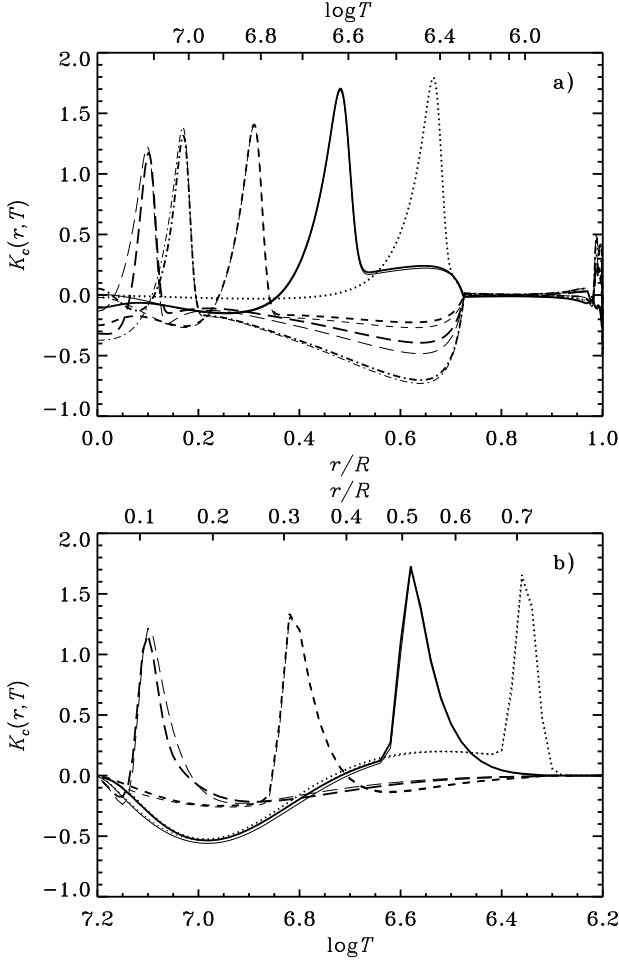


**Fig. 9.** Kernels  $K_c(r, T)$  relating the change in opacity to the sound-speed change (cf. Eq. 19). Heavy lines show kernels based on evolution calculation, while the thin lines were obtained from static models. **a** Kernels as a function of fractional radius  $r/R$  for  $\log T = 6.4$  (dotted line),  $\log T = 6.6$  (solid line),  $\log T = 6.8$  (short-dashed line),  $\log T = 7.0$  (dot-dashed line), and  $\log T = 7.1$  (long-dashed line). The upper abscissa shows  $\log T$ , corresponding to the lower abscissa. **b** Kernels as a function of  $\log T$ , for  $r/R = 0.70$  (dotted line),  $r/R = 0.50$  (solid line),  $r/R = 0.30$  (short-dashed line), and  $r/R = 0.10$  (long-dashed line). The upper abscissa shows  $r/R$ , corresponding to the lower abscissa

which kernels can reproduce the results of a large opacity change, by applying them to solar models with artificially reduced opacity values which simulate the effect of Weakly Massive Interacting Particles (WIMPs) (Christensen-Dalsgaard 1992).

Fig. 9 shows opacity kernels  $K_c(r, T)$  for sound speed, defined such that

$$\left(\frac{\delta_r c}{c}\right)(r) = \int K_c(r, T) \delta \log \kappa(T) d \log T. \quad (19)$$

**Table 3.** Properties of solar models with reduced core opacity, as well as the corresponding reference evolution model EW0

Model	$A$	$^{37}\text{Cl}$ neutrino flux (SNU)		$6D_0$ ( $\mu\text{Hz}$ )	
		Computed	kernels	Computed	kernels
EW0	0.0	8.89	–	9.169	–
SW1	0.2	4.87	4.76	8.023	8.071
SW2	0.4	2.96	2.55	7.034	7.105
EW1	0.2	4.59	4.61	8.395	8.439
EW2	0.4	2.67	2.39	7.697	7.767

These kernels were determined from the model changes discussed in Sect. 3.2 and are illustrated as functions of  $r$  and of  $T$ . Results for both static and evolution models are shown. As discussed in Sect. 4, the kernel for a given temperature  $T$  is localized in  $r$  fairly close to the position in the model corresponding to that temperature. Also, it is interesting that the kernels can be determined quite accurately from static models, except in the core where the evolution of the hydrogen abundance is substantially affected by the opacity modification. This provides some justification for the procedure adopted by Elliott (1995), which neglected possible evolutionary effects.

To illustrate the effects on important global properties of the model Fig. 10 shows kernels for the neutrino fluxes  $\Phi_\nu$  as well as the small frequency separation  $6D_0$  (cf. Eq. 6). Due to the high sensitivity of the neutrino fluxes to the opacity modifications, the neutrino kernels are defined specifically by

$$\delta \ln \Phi_\nu = \int K_\Phi(T) \delta \log \kappa(T) d \log T. \quad (20)$$

It is evident that these kernels correspond precisely, apart from a scaling, to the neutrino-flux differences shown in Fig. 4b. Also, it is striking that even for the neutrino flux there is little difference between the results for static and evolution models. In contrast, kernels for the small frequency separation, which depends strongly on the composition gradient in the core, cannot be estimated accurately from the static models.

To test these kernels, we use the models of Christensen-Dalsgaard (1992), with reduced core opacity. Specifically, the opacity modification was determined from

$$\log \kappa = \log \kappa_0 - Af(\log T), \quad (21)$$

where

$$f(\log T) = \begin{cases} \exp \left[ - \left( \frac{\log T - \log T_1}{\Delta \log T} \right)^2 \right], & \text{if } T < T_1 \\ 1 & \text{otherwise;} \end{cases} \quad (22)$$

as did Christensen-Dalsgaard (1992), we used  $\Delta \log T = 0.04$  and  $\log T_1 = 7.1$ . This form of  $f$  provides an opacity

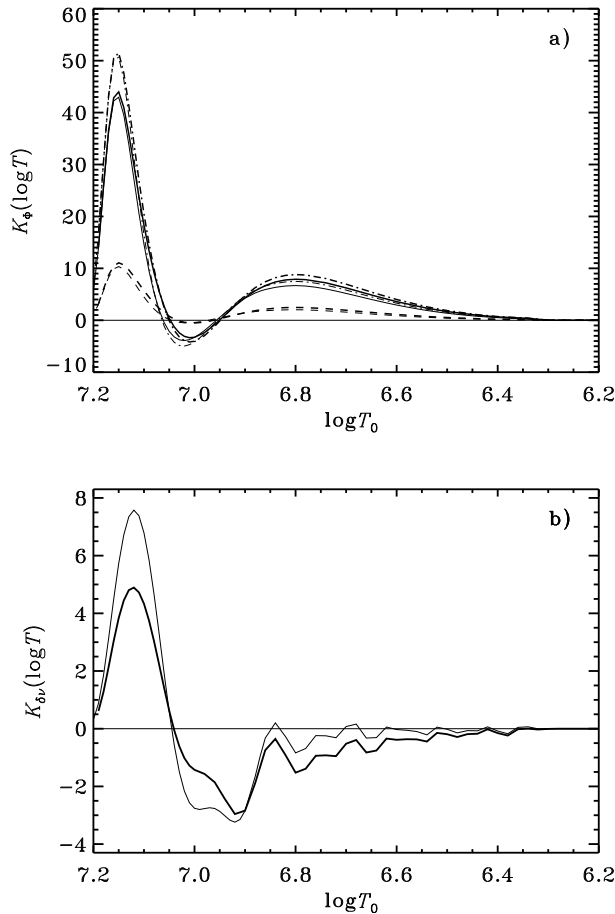


**Fig. 10.** Kernels for global model quantities. Heavy lines show kernels based on evolution calculation, while the thin lines were obtained from static models. **a** Kernels for logarithmic changes in the  $^{37}\text{Cl}$  and  $^{71}\text{Ga}$  capture rates (solid and dashed lines, respectively) and in the flux of  $^8\text{B}$  neutrinos (dot-dashed line) (cf. Eq. 20). **b** Kernels for the averaged small separation  $6D_0$  (cf. Eqs 6 and 7)

decrease over a well defined region in  $\log T$  with a continuous transition to zero at lower temperature. (Note that in these models the unmodified opacity  $\kappa_0$  was obtained using the Los Alamos Opacity Library of Huebner *et al.* 1977.) It was found that the neutrino flux was reduced by a factor of more than three for  $A = 0.4$  (see also Table 3).

Table 3 compares the values of the  $^{37}\text{Cl}$  neutrino flux and the small frequency separation computed for the models with reduced opacity with those estimated by means of the kernels shown in Fig. 10. It is evident that there is good agreement between the values of  $D_0$  for both  $A = 0.2$  and  $0.4$ . The agreement in neutrino flux is somewhat better for  $A = 0.2$ , the error being 10 – 15 % for  $A = 0.4$ . However, it is remarkable that linearized expressions of

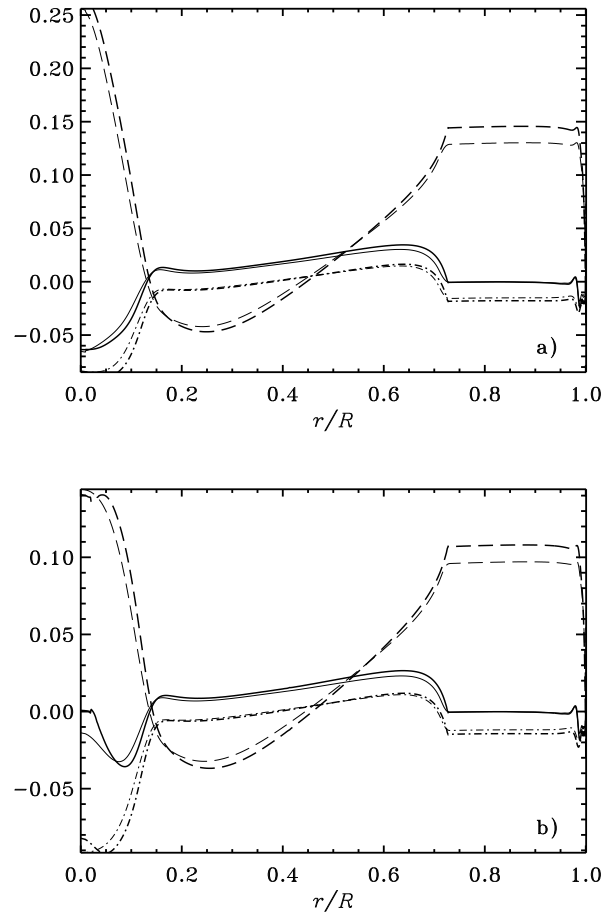


**Fig. 11.** Differences at fixed fractional radius  $r/R$  between models with opacity modification to simulate the effect of WIMPs (cf. Christensen-Dalsgaard 1992) and the corresponding reference models, in the sense (modified) – (reference). The thick lines represent the values obtained from the kernels while the thin lines show the original differences. Variables shown are  $\delta_r \ln c$  (solid line);  $\delta_r \ln \rho$  (dashed line);  $\delta_r \ln T$  (dash-dot line). Some properties of the models are provided in Table 3. **a** Differences between the modified static model SW2 and the reference model EW0. **b** Differences between the modified evolution model EW2 and the reference model EW0

the form given in Eq. (1) remain reasonably precise for a reduction in opacity by more than a factor of two.

To test the precision with which the kernels reproduce the structure of the model, Fig. 11 compares differences in  $c^2$  and  $\rho$  obtained from the kernels in Fig. 9 and the corresponding density kernels, with the actual model differences. Results are shown both for the static model SW2 and the evolution model EW2, both corresponding to  $A = 0.4$ . As before, the agreement is quite close both for evolution and for static models.

## 6. Conclusion

Our understanding of the solar internal structure has improved significantly over the last few years due to the rapid progress in helioseismology as well as in the construction of solar models with improved input physics. Although much of the knowledge has been obtained through inverse analysis, the starting point is always solar models; thus it is important to investigate the sensitivity of the solar structure to the input physics and to determine the presence of any region which is particularly sensitive to a specific parameter. Since the major uncertainties in the microphysics come from the opacity, we have focussed on the examination of the solar structure by means of a localised opacity change as a function of temperature.

The sensitivity of the solar structure was represented by kernels relating the opacity changes to neutrino flux, frequency separation at low degree as parametrised by  $D_0$  and the structure difference between modified and reference models. These kernels were subsequently used to derive the same parameters corresponding to a reduction in opacity by a factor of more than two in the models of Christensen-Dalsgaard (1992), simulating the effects of Weakly Interacting Massive Particles. We found that the kernels were remarkably successful in estimating the changes in the solar structure caused by even such a large change in the input physics.

A natural next step in this investigation is to study systematically how the oscillation frequencies are affected by opacity changes and also how well these frequency changes can be reproduced by kernels. Furthermore, in a preliminary analysis Tripathy, Basu & Christensen-Dalsgaard (1997) found that much of the current discrepancy between the helioseismically inferred solar sound speed and the sound speed of a standard solar model can be understood in terms of modest modifications to the opacity. More detailed analyses of this nature are now under way.

*Acknowledgements.* We thank S. Basu and J. Elliott for useful discussion as well as for comments on the manuscript. JC-D is grateful to the High Altitude Observatory for hospitality during much of the preparation of the paper. The work was supported in by Danish Natural Science Research Council, and by the Danish National Research Foundation through its establishment of the Theoretical Astrophysics Center. SCT acknowledges financial support from the Department of Science and Technology, Government of India.

## Appendix A: Some properties of convective envelopes

For convenience, we present some simple approximate properties of convective envelopes, which are useful for the interpretation of the numerical results in Sect. 4.2. Further details were provided by Christensen-Dalsgaard (1997). Note also that Baturin & Ayukov (1995, 1996)

carried out a careful analysis of the properties of convective envelopes and their match to the radiative interior.

In the convection zone the stratification departs substantially from being adiabatic only in a very thin region just below the photosphere. Thus the structure of the bulk of the convection zone is determined by the equation of hydrostatic equilibrium

$$\frac{dp}{dr} = -\frac{Gm\rho}{r^2} \quad (\text{A1})$$

( $G$  being the gravitational constant and  $m$  the mass interior to  $r$ ), and the relation

$$\frac{1}{\gamma} \equiv \frac{d \ln \rho}{d \ln p} \simeq \frac{1}{\gamma_1}. \quad (\text{A2})$$

To this approximation, the convection-zone structure therefore depends only on the equation of state, the composition and the constant specific entropy  $s$ , the latter being fixed by the mixing-length parameter  $\alpha_c$ . In practice, a more useful characterization of the bulk of the convection zone follows from noting that  $\gamma_1$  is approximately constant outside the dominant ionization zones of hydrogen and helium; then Eq. (A2) shows that  $p$  and  $\rho$  are related by

$$p \simeq K\rho^{\gamma_1}, \quad (\text{A3})$$

where the constant  $K$  is closely related to  $s$ . Assuming  $\gamma_1$  again to be constant and neglecting the mass in the convection zone, it is readily shown from Eqs (A1) and (A2) that  $u \equiv p/\rho = c^2/\gamma_1$  is given by

$$u \simeq GM \left(1 - \frac{1}{\gamma_1}\right) \left(\frac{1}{r} - \frac{1}{R^*}\right), \quad (\text{A4})$$

approximately valid in the lower parts of the convection zone (e.g. Christensen-Dalsgaard 1986; Dziembowski, Pamyatnykh & Sienkiewicz 1992; Christensen-Dalsgaard & Däppen 1992; Baturin & Mironova 1995); here  $M$  is the mass of the model and  $R^* \simeq R$ , its surface radius. From Eqs (A3) and (A4) we also obtain

$$p^{1-1/\gamma_1} \simeq K^{-1/\gamma_1} \frac{\gamma_1 - 1}{\gamma_1} GM \left(\frac{1}{r} - \frac{1}{R^*}\right). \quad (\text{A5})$$

Eq. (A4) indicates that  $u$ , and therefore  $c$ , depend little on the details of the physics of the model; in particular, if  $M$  and  $R$  are assumed to be fixed, as in the case of calibrated solar models,  $\delta_r u \simeq 0$ . This is confirmed by Figs 2 and 3, which show that  $\delta_r \ln c$  is very small in the bulk of the convection zone. From Eq. (A5) it furthermore follows that

$$\delta_r \ln p \simeq \delta_r \ln \rho \simeq -\frac{1}{\gamma_1 - 1} \delta \ln K \quad (\text{A6})$$

are approximately constant, again in accordance with Figs 2 and 3. Finally, assuming the ideal gas law, we have that

$$\delta_r \ln T \simeq \delta_r \ln \mu. \quad (\text{A7})$$

These relations may be used to investigate the changes in the model resulting from changes in the convection-zone parameters. Of particular interest are conditions at

the base of the convective envelope, defining the match to the radiative interior. Neglecting possible convective overshoot,  $\nabla_{\text{ad}} = \nabla_{\text{rad}}$ , the radiative temperature gradient, at this point. For calibrated models the luminosity  $L$  is unchanged; then  $\nabla_{\text{rad}} \propto \kappa p / T^4$ . Assuming also that  $\nabla_{\text{ad}}$  is constant and that the heavy-element abundance  $Z$  is fixed, we find that the change in the pressure  $p_{\text{cz}}$  at the base of the convection zone is related to the changes in  $K$  and the envelope hydrogen abundance  $X_s$  by

$$\delta \ln p_{\text{cz}} \simeq -\frac{4 - \tilde{\kappa}_T}{(4 - \tilde{\kappa}_T)(\gamma_1 - 1) - \gamma_1(\tilde{\kappa}_p + 1)} \delta \ln K - \frac{\gamma_1[(4 - \tilde{\kappa}_T)\mu_X - \tilde{\kappa}_X]}{(4 - \tilde{\kappa}_T)(\gamma_1 - 1) - \gamma_1(\tilde{\kappa}_p + 1)} \delta \ln X_s \quad (\text{A8})$$

(see also Christensen-Dalsgaard 1997); here

$$\tilde{\kappa}_p = (\partial \ln \kappa / \partial \ln p)_{T, X}, \quad \tilde{\kappa}_T = (\partial \ln \kappa / \partial \ln T)_{p, X}, \\ \tilde{\kappa}_X = (\partial \ln \kappa / \partial \ln X)_{p, T}, \quad \mu_X = (\partial \ln \mu / \partial \ln X)_Z.$$

Having obtained  $\delta \ln p_{\text{cz}}$ , the change in the depth of the convection zone can be determined from Eq. (A5) as

$$\delta \ln d_{\text{cz}} \simeq \frac{1}{\gamma_1} \frac{r_{\text{cz}}}{R} [\delta \ln K + (\gamma_1 - 1) \delta \ln p_{\text{cz}}], \quad (\text{A9})$$

where  $r_{\text{cz}}$  is the radius at the base of the convection zone. [Note that this relation differs from Eq. (11) of Christensen-Dalsgaard (1997). There it was assumed that the interior properties of the model were largely unchanged while the surface radius was allowed to change; this is the case relevant, for example, to the calibration of solar models to have a specific radius. Here we have kept  $R$  fixed and the change in  $d_{\text{cz}}$  corresponds to changes in the properties of the radiative interior of the model.]

It is of some interest to compare these simple relations with the numerical results obtained for the envelope models listed in Table 2. To do so, we first need to relate the change in  $K$  to the changes in  $\alpha_c$  and  $X_s$ . From the results in Table 2

$$\left( \frac{\partial \ln K}{\partial \ln \alpha_c} \right)_{X_s} \simeq -1.40, \quad \left( \frac{\partial \ln K}{\partial \ln X_s} \right)_{\alpha_c} \simeq 1.90. \quad (\text{A10})$$

As discussed by Christensen-Dalsgaard (1997), the relation between  $\alpha_c$  and  $K$ , at fixed composition, follows simply from the properties of the mixing-length theory; the result of such an analysis, using the properties of the reference envelope model En1, agrees quite closely with the value given above. It is less straightforward to derive a simple expression for the relation between  $\delta \ln K$  and  $\delta \ln X_s$ .

To evaluate the changes in  $p_{\text{cz}}$  and  $d_{\text{cz}}$ , we need the derivatives of  $\kappa$  and  $\mu$ . At the base of the convection zone in the reference envelope En1 we have the following values:  $\tilde{\kappa}_p = 0.63$ ,  $\tilde{\kappa}_T = -3.70$ ,  $\tilde{\kappa}_X = -0.16$ , and  $\mu_X = -0.54$ . Thus, from Eq. (A8) we obtain  $\delta \ln p_{\text{cz}} \simeq -3.20 \delta \ln K + 2.99 \delta \ln X_s$ , and hence, from Eq. (A9),

$$\delta \ln d_{\text{cz}} \simeq -0.49 \delta \ln K + 0.87 \delta \ln X_s. \quad (\text{A11})$$

Using also Eqs (A10) we find

$$\delta \ln d_{\text{cz}} \simeq 0.69 \delta \ln \alpha_c - 0.07 \delta \ln X_s. \quad (\text{A12})$$

For comparison, the results in Table 2 give

$$\left( \frac{\partial \ln d_{\text{cz}}}{\partial \ln \alpha_c} \right)_{X_s} \simeq 0.72, \quad \left( \frac{\partial \ln d_{\text{cz}}}{\partial \ln X_s} \right)_{\alpha_c} \simeq -0.18. \quad (\text{A13})$$

Evidently, the  $\alpha_c$ -derivative is in reasonable agreement with Eq. (A12); although the agreement appears less satisfactory for the derivative with respect to  $X_s$ , it should be noticed that small coefficient in Eq. (A12) arises from near cancellation between the contributions from the two terms in Eq. (A11).

## References

- Bahcall J. N., 1989, *Neutrino Astrophysics*, Cambridge University Press, Cambridge
- Bahcall J. N., Bahcall N. A., Ulrich R. K., 1969, *ApJ* 156, 559
- Bahcall J. N., Ulrich R. K., 1988, *Rev. Mod. Phys.* 60, 297
- Baturin V. A., Ayukov S. V., 1995, *AZh* 72, 549 (Engl. translation: *Astronomy Reports* 39, 489)
- Baturin V. A., Ayukov S. V., 1996, *AZh* 73, 259 (Engl. translation: *Astronomy Reports* 40, 233)
- Baturin V. A., Mironova I. V., 1995, *AZh* 73, 120 (Engl. translation: *Astronomy Reports* 39, 105)
- Böhm-Vitense E., 1958, *Z. Astrophys.* 46, 108
- Christensen-Dalsgaard J., 1982, *MNRAS* 199, 735
- Christensen-Dalsgaard J., 1986, in: *Seismology of the Sun and the Distant Stars*, ed. D. O. Gough, Dordrecht, Reidel, p. 23
- Christensen-Dalsgaard J., 1988, in: *Seismology of the Sun and Sun-like Stars*, eds V. Domingo, E. J. Rolfe, ESA SP-286, ESTEC, Noordwijk, p. 431
- Christensen-Dalsgaard J., 1992, *ApJ* 385, 354
- Christensen-Dalsgaard J., 1997, in: *it Solar Convection and Oscillations and their Relationship: Proc. SCORE'96*, Aarhus, May 1996, eds F. P. Pijpers, J. Christensen-Dalsgaard, C. S. Rosenthal, in the press
- Christensen-Dalsgaard J., Berthomieu G., 1991, in: *Solar Interior and Atmosphere*, eds A. N. Cox, W. C. Livingston, M. Matthews Space Science Series, University of Arizona Press, Tucson, p. 401
- Christensen-Dalsgaard J., Däppen W., 1992, *A&AR* 4, 267
- Christensen-Dalsgaard J., Thompson M. J., 1991, *ApJ* 367, 666
- Christensen-Dalsgaard J., Däppen W., Ajukov S. V. *et al.*, 1996, *Sci* 272, 1286
- Dziembowski W. A., Pamyatnykh A. A. & Sienkiewicz R., 1992, *Acta Astron.* 42, 5
- Eggleton P. P., Faulkner J., Flannery B. P., 1973, *A&A* 23, 325
- Elliott J. R., 1995, *MNRAS* 277, 1567
- Gough D. O., 1985, *Solar Phys.* 100, 65
- Huebner W. F., Merts A. L., Magee N. H., Argo M. F., 1977, Los Alamos Scientific Laboratory Report LA-6760-M.
- Iglesias C. A., Rogers F. J. & Wilson B. G., 1992, *ApJ* 397, 717
- Kippenhahn R. & Weigert A., 1990, *Stellar structure and evolution*, Springer-Verlag, Berlin
- Korzennik S. G. & Ulrich R. K., 1989, *ApJ* 339, 1144
- Parker P. D., 1986, in: *Physics of the Sun*, eds P. A. Sturrock, T. E. Holzer, D. Mihalas, Ulrich, R. K., Dordrecht, Reidel, p. 15
- Saio H., 1992, *MNRAS* 258, 491

Tripathy S. C., Basu S. & Christensen-Dalsgaard J., 1997, in:  
Poster Volume; Proc. IAU Symposium No 181: Sounding  
Solar and Stellar Interiors, eds F. X. Schmider, J. Provost,  
Nice Observatory, in the press